

ORIGINAL ARTICLE

Quantitative analysis of the phase-separated structure and mechanical properties of acrylic copolymer/epoxy thermosetting resin composites

Isao Ichikawa^{1,2}, Toshio Sugizaki¹, Shuichi Akasaka² and Shigeo Asai²

The effects of thermal curing reactivity on the phase-separated structures of acrylic copolymer/epoxy thermosetting resin composites containing various accelerator amounts were investigated to elucidate their phase separation behavior. These composites exhibited a sea-island structure, in which the island size decreased as the amount of accelerator increased. The island diameter distribution was represented as a lognormal plot. Island formation is explained by the law of proportionate effect. As observed during the last stage of phase separation via spinodal decomposition, small domains formed prior to coalescing. The effects of material composition on the phase structures and mechanical properties of acrylic copolymer/epoxy thermosetting resin composites were also examined. The morphologies varied depending on the components, and in particular, the total island area fractions and fracture surface shapes after the tensile tests differed. A small fraction of island area resulted in a lower fracture surface roughness and higher mechanical strength, indicating that in stronger composites, many epoxy components remained in the acrylic copolymer-rich sea phases. In addition, the destruction of resin composites was propagated through phase boundaries because the network formation states of the sea and island phases do not significantly differ.

Polymer Journal advance online publication, 28 October 2015; doi:10.1038/pj.2015.68

INTRODUCTION

Epoxy thermosetting resins are used as adhesives in many industrial applications and enabled technological advances in organic–inorganic hybrid devices. In the assembly of semiconductor components, many compounds have been used in the devices and bonded using various techniques. For example, metal silicon dies adhere to printed circuit boards due to the organic polymer-based die bond materials. Adhesion durability is important for device reliability. In particular, their manufacturing processes require high-adhesive strength at temperatures exceeding 250 °C.¹ Therefore, epoxy thermosetting systems have been applied to adhesive matrix resins to satisfy such requirements.^{2,3} These epoxy thermosetting systems are immiscible with other components, such as thermoplastic resins, and generate phase-separated structures of micrometer sizes.^{4–6} Several studies regarding the phase separation phenomena of epoxy composites using a light scattering method have been reported. Yamanaka and Inoue⁷ evaluated the phase separation of an epoxy thermosetting resin mixture consisting of the diglycidyl ether of bisphenol A epoxy resin, diaminodiphenylmethane as a curing agent, and poly(ether sulfone). The compound was a single-phase mixture in the early stage of curing. As the curing reaction progressed, phase separation occurred along with an increase in the molecular weight of the epoxy thermosetting resin. At this stage, the composite phase diagram contained a lower critical solution temperature (LCST), and a two-phase region should

prevail in the phase diagram as the molecular weight increases during curing. The thermodynamic change in the phase diagram with epoxy chain extension results in a phase-separated structure with a change in the quench depth, which is the difference in temperature between the LCST and the reaction temperature. The cured composites exhibited an interconnected globule structure and higher adhesive strength than that of neat epoxy resin. These structures, which have an essential role in their mechanical strength, form via spinodal decomposition as the phase diagram changes.^{7,8}

Therefore, physical phenomena, such as phase separation exhibited by composite materials containing an epoxy component, are required to account for many factors, which have thermodynamic and kinetic aspects.⁹ In addition, the adhesion mechanism is due to the chemical interaction with the adherend and the strength of the adhesive itself. The latter is very important for thick adhesives and affected by phase-separated structure. Therefore, the evaluation of the phase structure of epoxy thermosetting systems is important for advanced material design.

In this study, the phase structure and mechanical properties of composites that are primarily composed of epoxy thermosetting resins and undergo phase separation were investigated. Specifically, the influence of resin reactivity on the phase structure was evaluated for acrylic copolymer/epoxy thermosetting resin composites. In addition, the effects of material composition on the phase structure and

¹Structural Analysis Laboratory, LINTEC Corporation, Saitama, Japan and ²Department of Chemistry and Materials Science, Tokyo Institute of Technology, Tokyo, Japan

Correspondence: Associate Professor S Asai, Department of Chemistry and Materials Science, Tokyo Institute of Technology, 2-12-1-S8-43, Ookayama, Meguro-ku, Tokyo 152-8550, Japan.

E-mail: asai.s.aa@m.titech.ac.jp

Received 2 May 2015; revised 14 June 2015; accepted 2 July 2015

mechanical strength were investigated. Then, the phase-separated structure of the composites was examined using two analytical techniques with scanning probe microscopy (SPM) images. First, the distribution of the diameter and the nearest-neighbor distance between the centers of island domains were derived by particle size analysis. Second, the islandicity and correlation length of the phase structure were evaluated by two-dimensional fast-Fourier transform (2D-FFT) analysis.¹⁰ These quantitative analyses of the phase structure provided insight into the phase separation process and physical strength development of acrylic copolymer/epoxy thermosetting resin composites.

MATERIALS AND METHODS

Sample preparation

The epoxy thermosetting resin and acrylic copolymer molecular structures are shown in Figure 1 and their compositions are shown in Table 1. The epoxy thermosetting system was prepared by mixing four types of epoxide compounds: the diglycidyl ether of bisphenol A epoxy resin (JER-828, Mitsubishi Chemical Corporation, Tokyo, Japan, epoxy equivalent: 184–194 g eq⁻¹, viscosity: 12–15 Pa s (25 °C)), a multifunctional epoxy resin (Figure 1a, EPPN-502H, Nippon Kayaku Co., Ltd., Tokyo, Japan, epoxy equivalent: 158–178 g eq⁻¹, mp.: 60–72 °C), a dicyclopentadiene epoxy resin (Figure 1b, HP-7200H, DIC Corporation, Tokyo, Japan, epoxy equivalent: 274–286 g eq⁻¹, mp.: 88–98 °C), and an *o*-cresol novolac epoxy resin (Figure 1c, EOCN-104S, Nippon Kayaku Co., Ltd., epoxy equivalent: 218 g eq⁻¹, mp.: 92 °C). Phenol novolac (Figure 1d, PAPS-PN4, Asahi Organic Chemicals Industry Co., Ltd., Tokyo, Japan, hydroxyl equivalent: 104 g eq⁻¹, mp.: 111 °C) was used as a curing agent. 4,5-Dihydroxymethyl-2-phenylimidazole (Figure 1e, 2PHZ-PW, Shikoku Chemicals Corp., Kagawa, Japan, $M_w = 188$, mp.: 190–202 °C) was used as an accelerator. The four types of epoxide

compounds were mixed in a 4:4:2:1 ratio in an epoxy equivalent amount. The equivalent ratio of hydroxyl groups in the curing agent to the epoxide groups was adjusted to 0.85, and 5.1 mmol of accelerator was added for 1 mol of hydroxyl groups in the curing agent.

The epoxy system was mixed with poly(methyl acrylate) (MA, $M_w = 280\,000$, $M_w/M_n = 2.9$) in 2-butanone. The resulting mixture (i.e., a 70 wt% solution) was cast and dried on a polyethylene terephthalate (PET) film has a release layer. The 40 μm thick prepared film was cured at 120 °C for 1 h and at 175 °C for 2 h (standard conditions) to prepare the MA/E4_1.0 sample. Samples containing one-quarter and four times the accelerator amount were also prepared to investigate the effects of the reactivity of thermal curing on the phase separation (MA/E4_0.25, MA/E4_4.0). In the sample names, the first two characters correspond to the acrylic copolymer component, the next two characters indicate the number of epoxide types in the resin, and the last characters indicate the relative amount of accelerator.

Table 1 Composition of samples

Sample name	Acrylic polymer ^a	Epoxy thermosetting resin system	Accelerator amount
MA/E4_1.0	MA	4 types of epoxy resin ^b	Control ^c
MA/E4_0.25	MA	4 types of epoxy resin	× 0.25
MA/E4_4.0	MA	4 types of epoxy resin	× 4.0
MH/E4_1.0	MH	4 types of epoxy resin	Control
MG/E4_1.0	MG	4 types of epoxy resin	Control
MH/E2_1.0	MH	2 types of epoxy resin	Control

^aThe ratio of the acrylic polymer and epoxy thermosetting resins is 30:70 in weight.

^bEquivalent ratio of the hydroxyl group in the curing agents to epoxide group was adjusted to 0.85.

^c5.1 mmol for 1 mol of hydroxyl groups in the curing agents.

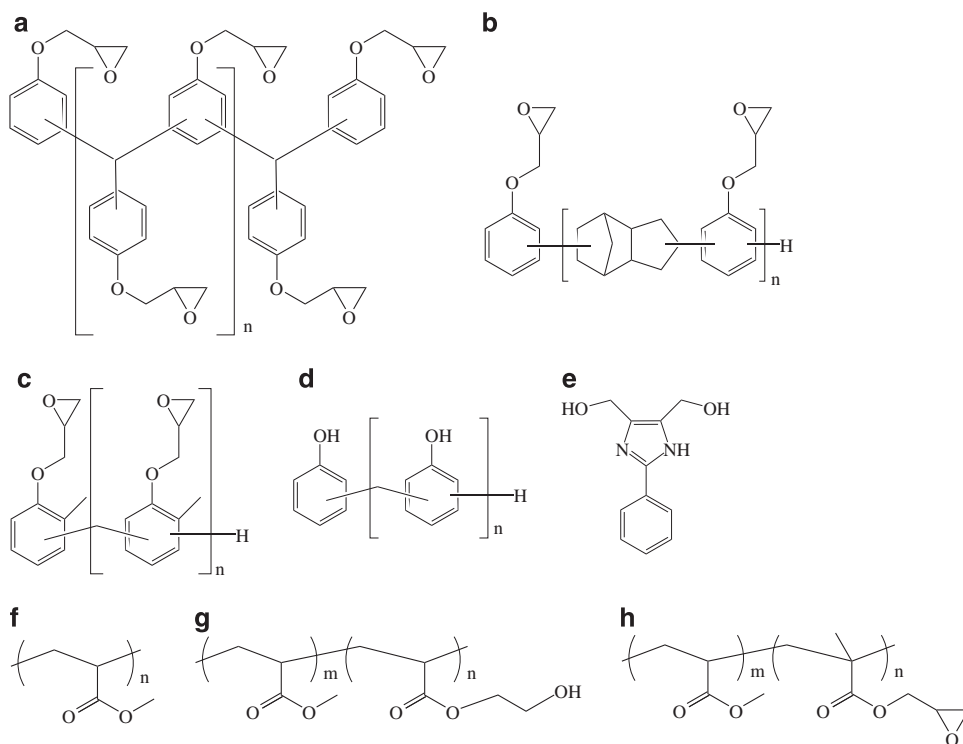


Figure 1 Epoxy thermosetting resin and acrylic polymer component for each sample. (a) Multifunctional epoxy resin, (b) dicyclopentadiene epoxy resin, (c) *o*-cresol novolac epoxy resin, (d) phenol novolac curing agent, (e) imidazole type accelerator ([4-(hydroxymethyl)-2-phenyl-1H-imidazol-5-yl]methanol), (f) methyl acrylate homopolymer (MA), (g) poly[(methyl acrylate)-*co*-(2-hydroxyethyl acrylate)] ($m:n = 85:15$ mol%; MH), and (h) poly[(methyl acrylate)-*co*-(glycidyl methacrylate)] ($m:n = 85:15$ mol%; MG).

In addition, three samples consisting of different acrylic copolymers and epoxy resin mixtures were prepared to investigate the effects of material composition on phase structure and mechanical strength. The first composite (MH/E4_1.0) consisted of 85:15 (mol/mol) methyl acrylate/2-hydroxyethyl acrylate copolymer (poly[(methyl acrylate)-*co*-(2-hydroxyethyl acrylate)]), MH, $M_w = 370\,000$, $M_w/M_n = 4.2$) and the original epoxy system (E4_1.0). The second sample (MG/E4_1.0) consisted of 85:15 methyl acrylate/glycidyl methacrylate copolymer (poly[(methyl acrylate)-*co*-(glycidyl methacrylate)]), MG, $M_w = 270\,000$, $M_w/M_n = 4.4$) and the E4_1.0 epoxy system. The third composite (MH/E2_1.0) combined the MH acrylate copolymer and two types of epoxide compounds as a thermosetting resin (E2_1.0). The E2_1.0 epoxy system is composed of the diglycidyl ether of bisphenol A epoxy resin and *o*-cresol novolac epoxy resin in a 3:8 ratio in an epoxy equivalent amount, and the curing agent and accelerator were added in the same manner as with the original epoxy system (E4_1.0). The last sample had a glycidyl group density of $2.30 \times 10^{-3} \text{ mol g}^{-1}$, which is slightly less than that of MH/E4_1.0 ($2.41 \times 10^{-3} \text{ mol g}^{-1}$).

All of the acrylic polymers were provided by the Nippon Synthetic Chemical Industry Co., Ltd (Osaka, Japan).

Measurements and analyses

The phase structures of the sample surfaces were investigated using SPM images in the $1.2 \times 1.2 \mu\text{m}^2$ and $20 \times 20 \mu\text{m}^2$ ranges. The scanning was conducted in tapping mode using a SPA-300HV (Hitachi High-Tech Science Corporation, Tokyo, Japan) and a SI-DF40 cantilever at a resonance frequency of ca. 320 kHz.

The SPM images were analyzed using two methods. In the first approach, the particle size distribution was evaluated using the topological image. To prepare the specimens for this analysis, the acrylic polymer component (or acrylic polymer-rich phase) that was isolated on the surface was dissolved by immersion in excess 2-butanone for 60 h. The height distribution of the sample surface after immersion exhibited one minimum surrounded by two peaks. Therefore, the SPM topological images could be converted into binary images with a height distribution profile, wherein the minimum served as the threshold dividing the two phase areas. The distribution of the particle diameter and the nearest-neighbor distance between the centers of island domains were determined from these binary images using our original software.

In the second method, the structural periodicity was assessed using the SPM phase images. These images were processed by 2D-FFT using the Image-J software (NIH open source).^{11,12}

The light scattering measurements were performed using a DYNA3000 instrument (Otsuka Electronics Co. Ltd., Osaka, Japan) to investigate the phase separation progress with the bulk structural periodicity. The measurement chamber was set horizontally on the light scattering stage, and the specimen was irradiated vertically with a He–Ne gas laser ($\lambda = 632.8 \text{ nm}$). The goniometer was positioned at $2\theta = 60^\circ$, which corresponded to the light beam center scattered from the film under a parallel polarized (Vv) optical alignment. The scattering pattern was acquired using a charge-coupled device (CCD) camera from 48° to 72° , resulting in a one-dimensional (1D) light scattering profile. The angles were accurately corrected using sample refractive indices.

The specimens were prepared by curing a MA/E4_1.0 film under various conditions. The films were cured on an $8 \times 8 \times 0.15 \text{ mm}^3$ glass slide at 125°C for 30 min (condition 1) or 1 h (condition 2) and heated to 175°C beyond condition 2 (condition 3) and maintained for 2 h (condition 4, standard condition). The heating rate was 3°C min^{-1} for each temperature process.

The heat of reaction, molecular mobility (before and after curing), and local surface elastic modulus were measured to characterize the network state formed during curing.

To estimate the number of covalent bonds formed by the epoxy thermosetting resins, the heats of reaction were measured with the samples prior to curing. The measurements were performed using a Pyris 1 heat-compensation differential scanning calorimetry apparatus (Perkin Elmer, Inc., Waltham, MA, USA) under nitrogen atmosphere at a heating rate of $10^\circ\text{C min}^{-1}$. The onset temperatures and heats were derived and compared.¹³

The storage moduli on the shear mode at 1.0 Hz with the MA/E4_1.0 and MH/E4_1.0 samples prior to curing were measured at 125°C to compare the

molecular mobility at the curing temperature using an ARES-G2 (TA instrument, New Castle, DE, USA).

The spin–spin relaxation time (T_2) was evaluated by pulse ^1H nuclear magnetic resonance using a Minispec mq20 instrument (Bruker BioSpin K.K., Kanagawa, Japan) at 20 MHz to assess the molecular mobility after curing. The pulse ($90^\circ_x - \tau - 90^\circ_y$; solid echo method)¹⁴ and spin echo pulse ($90^\circ_x - \tau - (180^\circ_y - 2\tau -)$; Carr–Purcell–Meiboom–Gill (CPMG) method)¹⁵ sequences were adopted. The former pulse sequence has the advantage of avoiding the dead time effect after the pulse, and the latter spin echo pulse can eliminate the effect from the inhomogeneity of the magnetic field. Therefore, the fast decay of magnetization with low-mobility proton components was measured by the solid echo method, and the slow decay of magnetization with high-mobility components was measured using the CPMG method.

The free induction decay (FID) signal obtained by the solid echo method was split into one Gaussian and two exponential components.^{16–18}

$$M(t) = M_1 \exp\{-1/2[t/T_2(1)]^2\} + M_2 \exp[-t/T_2(2)] \\ + M_3 \exp[-t/T_2(3')] \quad (1)$$

where M_i and $T_2(i)$ are the initial magnetization intensity and relaxation time of the i^{th} component, respectively. The dashed number in the third term represents a ‘provisional value’ for a proton component exhibiting a longer relaxation time because it is divided by the CPMG method.

Similarly, the FID signal measured by the CPMG method was decomposed into three exponential terms as follows:

$$M(t) = M_3 \exp[-t/T_2(3)] + M_4 \exp[-t/T_2(4)] + M_5 \exp[-t/T_2(5)] \quad (2)$$

Each component fraction (F_i) was calculated using:

$$\begin{cases} F_i = \frac{M_i}{\sum_{j=1}^5 M_j} & (\text{for } i = 1, 2) \\ F_i = \frac{M_i}{\sum_{j=1}^5 M_j} \cdot \frac{M_i}{\sum_{k=3}^5 M_k} & (\text{for } i = 3, 4, 5). \end{cases} \quad (3)$$

The measurements were conducted at 95°C , which is intermediate between the glass transition temperatures of the simple epoxy thermosetting resin after curing under standard conditions (ca. 150°C) and that of the simple acrylic copolymer (ca. 35°C) used in this study.

The local surface elastic modulus was estimated according to the Hertz theory using the SPM force curve.^{19,20} The force curves were measured with the same equipment and cantilever as that employed for the morphology observations. The indentation depth and rate were set to 50 nm and 10 nm s^{-1} , respectively. The elastic moduli were calculated by fitting equation (4) to the force curves for the sea and island areas.

$$F = \frac{4E}{3(1-\nu^2)} R^{1/2} \delta^{3/2} \quad (4)$$

where δ and F are the sample deformation and exerted force derived from the piezo scanner displacement, cantilever deflection and spring constant ($k = 53 \text{ N m}^{-1}$). R is the cantilever tip diameter (10 nm), E is the elastic modulus and ν is Poisson’s ratio with values of 0.43, 0.47, 0.38 and 0.48 for MA/E4_1.0, MH/E4_1.0, MG/E4_1.0 and MA/E2_1.0, respectively. These value were derived from the ratio of the strain between the longitudinal and transverse direction observed using an advanced video extensometer at the tensile test at a pulling rate of 1.0 mm min^{-1} using a 5567 series Universal testing machine (Instron, Norwood, MA, USA) at 23°C .

The tensile strengths were measured at 250°C at a 5.0 mm min^{-1} pulling rate using a 5581 series Universal testing machine (Instron) equipped with a thermostatic chamber. After breaking, the fracture surfaces were observed by scanning electron microscopy (VE-9800, KEYENCE, Osaka, Japan), and their degree of roughness (R_a) in the $2 \times 2 \mu\text{m}^2$ areas was measured by SPM, as previously mentioned.

RESULTS AND DISCUSSION

Influence of curing accelerator amount on morphology

The morphologies of the acrylic copolymer/epoxy thermosetting resin composite were examined by SPM phase imaging (Figure 2a). The top and bottom images in Figure 2 correspond to $10 \times 10 \mu\text{m}^2$ area

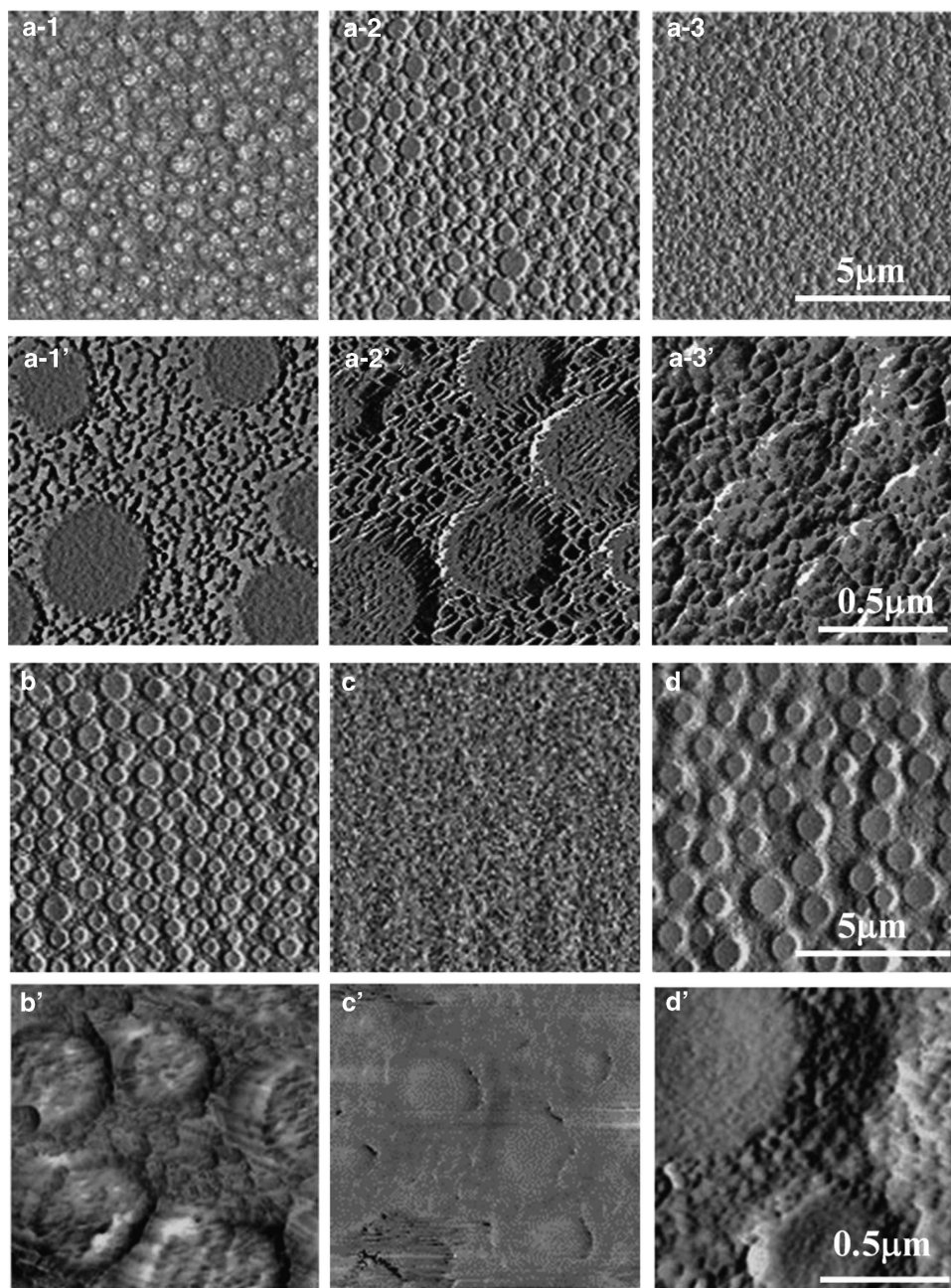


Figure 2 Scanning probe microscopy phase image of (a-1, a-1') MA/E4_0.25, (a-2, a-2') MA/E4_1.0 and (a-3, a-3') MA/E4_4.0, which have different amounts of the accelerator in the thermal curing systems and (b, b') MH/E4_1.0, (c, c') MG/E4_1.0 and (d, d') MH/E2_1.0, which have different acrylic copolymer components and different epoxy thermosetting resin components.

micrographs and their magnifications, respectively. All of the samples exhibited sea-island structures wherein the island domains were within the submicron range.

The distribution of the particle diameter and the nearest neighbor distance between the centers of island domains were obtained from the binarized SPM image (Figure 3). The lines in each figure represent fitting results to the lognormal distribution:

$$f(x) = \frac{1}{x\sigma\sqrt{2\pi}} \exp\left[-\frac{(\ln x - \mu)^2}{2\sigma^2}\right] \quad (5)$$

where μ and σ are the mean and standard deviation (s.d.) of the normal distribution for $\ln x$, respectively. All of the frequency data matched the lognormal distribution curve. In addition, the domain particle diameter and the nearest neighbor distance between particles decreased with increasing curing accelerator amount.

The mean (m) and mode (p) values were derived from fitting to equation (5) and

$$m = \exp[\mu + \sigma^2/2] \quad (6)$$

Their difference normalized by $p((m-p)/p)$ was also calculated (Table 2).

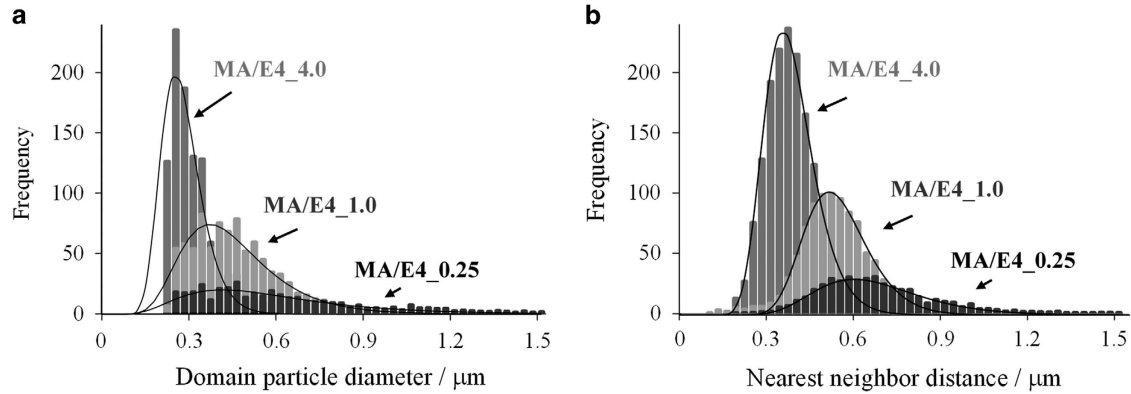


Figure 3 Distribution of (a) domain particle diameter and (b) nearest neighbor distance of the scanning probe microscopy topology images of the samples with different amounts of accelerator.

Table 2 Fitting parameter with distribution analysis to the lognormal function and total area fraction of island

	Domain particle diameter (μm)			Nearest neighbor distance (μm)			Total fraction of islands area (%)
	m	p	$(m-p)/p$	m	p	$(m-p)/p$	
MA/E4_0.25	0.60	0.42	0.43	0.66	0.66	0.00	49.5
MA/E4_1.0	0.45	0.36	0.25	0.53	0.51	0.04	40.3
MA/E4_4.0	0.28	0.24	0.17	0.37	0.36	0.03	25.3
MH/E4_1.0	0.69	0.54	0.28	0.75	0.69	0.09	33.3
MG/E4_1.0	0.29	0.24	0.21	0.47	0.42	0.12	31.7
MH/E2_1.0	1.17	0.63	0.86	1.28	1.14	0.12	48.9

The mean value (m), the mode value (p) and the difference between them normalized by p ($(m-p)/p$).

An $(m-p)/p$ value of 0 signifies a normal distribution. For the nearest-neighbor distance between particles, the m - and p -values were very close, which indicates a normal distribution. However, for the domain particle diameter, $(m-p)/p$ increased with decreasing amount of accelerator. Therefore, the domain size distribution of composites containing smaller amounts of accelerator significantly deviated from the normal distribution. When the phenomenon occurs spontaneously, the physical quantity that represents this phenomenon has a normal distribution and is an independent variable. By contrast, when a physical quantity displays the lognormal distribution, a physical behavior may obey the law of proportionate effect, wherein the physical quantity proportionally changes in response to a stimulus with the physical quantity of the previous stage. In this experiment, fine island domains were generated prior to growing and coalescing according to this law.²¹

The 2D-FFT images (Figures 4a–c) were obtained from the SPM micrographs. The distance from the image center represents the wavenumber absolute value (q), which is inversely proportional to the periodic length. Each image shows a white concentric annular area around its center, indicating the presence of structural periodicity that extends to the peripheral portion of the image for the accelerator-rich sample (MA/E4_4.0).

These 2D-FFT images were radially averaged to yield 1D intensity profiles (Figure 4d) and correlation lengths (l_m). The 1D profiles were derived from more than six 2D-FFT images for each sample and

averaged. These profiles exhibit a peak with an intensity that increased for samples with a smaller accelerator content. The structural periodicity increased when the island domain was larger.

The l_m values (Table 3) were calculated using the q_{peak} values as follows:

$$l_m = 2\pi/q_{\text{peak}} \quad (7)$$

These l_m values correspond to the nearest-neighbor distance between particles (Table 2) and follow the same tendency toward reactivity. Specifically, l_m increased as the accelerator content decreased. This behavior indicates that the structural periodicity results from the island's spatial position. In addition, the thermal reaction of the epoxy thermosetting resin acts as a driving force for the phase separation, and the thermal reaction could suppress the phase separation, leading to fixing the structure at the early stage of decomposition. Therefore, the phase structure of MA/E4_4.0, which has a high accelerator content and exhibits high reactivity, represents 'the pseudo in-progress state of phase formation' of MA/E4_0.25.

The light scattering patterns in the 2θ range between 48° and 72° ($q = 6.8\text{--}13 \mu\text{m}^{-1}$) and the 1D scattering intensity profiles are shown in Figure 5. A high-intensity region in the scattering patterns was observed from ~ 10.5 to $11.0 \mu\text{m}^{-1}$ for the samples cured under conditions 3 and 4, corresponding to the peaks exhibited by these samples in their 1D profiles. This peak became clearer, and q_{peak} decreased as the heat curing progresses, suggesting that higher periodicity and longer periodic structures accompany the development of the curing process. Ohnaga *et al.* evaluated the phase separation phenomena via spinodal decomposition with an epoxy composite using kinetic diffusion equation presented by Cahn–Hilliard, whereby the diffusion coefficient is defined as the product of the molecule mobility and second-order differential of the free energy function.⁸ The Flory–Huggins equation was employed as the free-energy function to represent the thermodynamic steady state. When the quench depth increased at isothermal demixing, the diffusion coefficient increased, and the structural coarsening was suppressed. Therefore, the peak angle of the scattering profile remains constant during the light scattering measurement. However, when the quench depth changing rate (quench rate) is very small, the coarsening process is observed.

In our experiment, the phase separation phenomenon with a small quench rate will occur, and the two-phase region should gradually prevail with the low reactivity and low-molecule mobility of the epoxy thermosetting system.

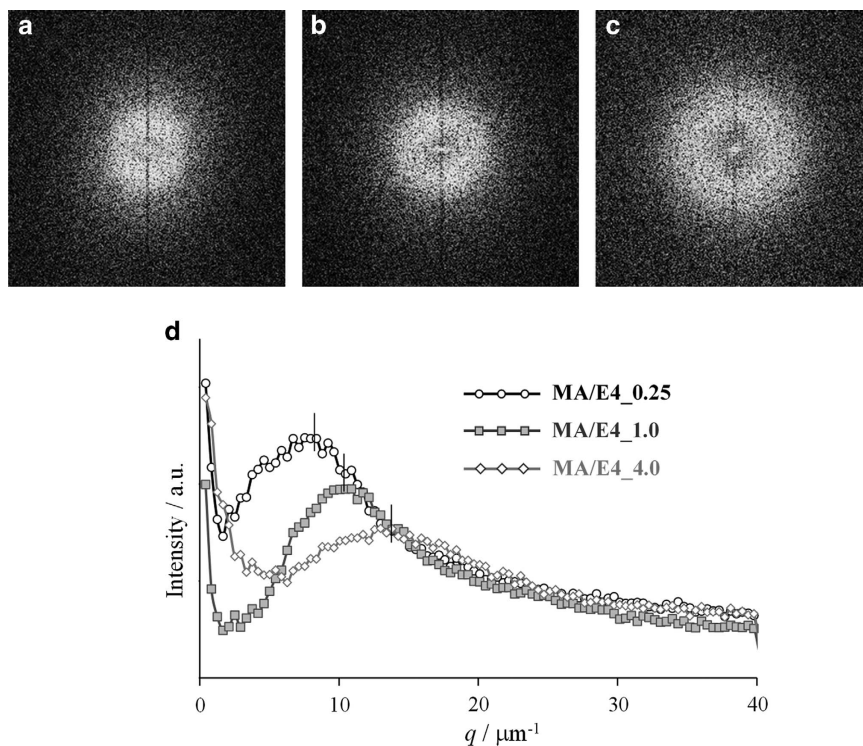


Figure 4 Images after two-dimensional fast-Fourier transform with the scanning probe microscopy phase image of (a) MA/E4_0.25, (b) MA/E4_1.0 and (c) MA/E4_4.0 as well as (d) one-dimensional intensity distribution profile. a.u., arbitrary unit.

Table 3 q -value at peak intensity (q_{peak}) on the 1D intensity profile derived from 2D-FFT analysis and correlation length (l_m)

	$q_{\text{peak}} (\mu\text{m}^{-1})$	$l_m (\mu\text{m})$
MA/E4_0.25	8.4	0.75
MA/E4_1.0	10.9	0.58
MA/E4_4.0	13.8	0.45
MH/E4_1.0	8.0	0.79
MG/E4_1.0	13.0	0.48
MH/E2_1.0	4.2	1.50

Abbreviations: 1D, one dimensional; 2D-FFT, two-dimensional fast-Fourier transform.

It is important to note that the noises in the profiles are large due to a low-scattering intensity, and this low intensity indicates the deficient decomposition of each component.

The correlation lengths were estimated using q_{peak} in the same manner as that employed in the 2D-FFT image analysis. The sample cured under condition 4 exhibited an l_m value of $0.60 \mu\text{m}$, which is in agreement with the result from 2D-FFT image analysis. Based on light scattering, which provides bulk structure information, the enhanced periodicity with the thermal reaction is also consistent with these image analysis results. Therefore, the surface structure observed by SPM also formed throughout the bulk.

Influence of the composition on the phase-separated structures and mechanical properties

The SPM phase images (Figures 2b–d) indicate that all of the samples exhibit phase-separated structures but with different morphologies, especially for sample MG/E4_1.0, for which the phase-separated structure has an ambiguous border.

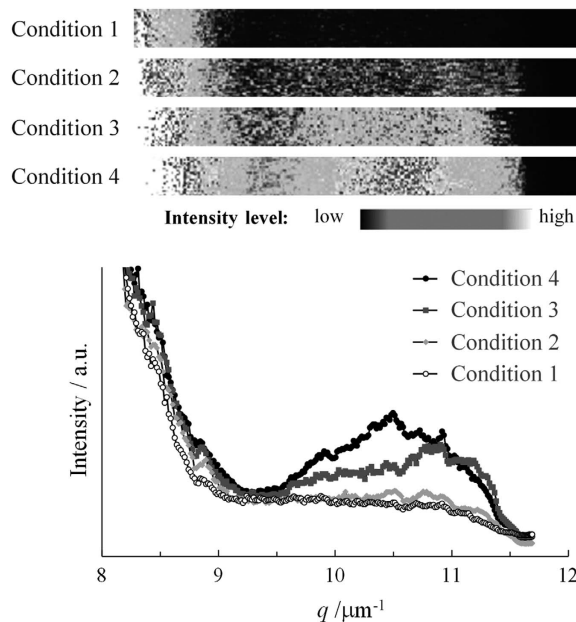


Figure 5 Light scattering pattern of cured MA/E4_1.0 and intensity profile.

The m , p and $(m-p)/p$ values were derived in the same manner as the evaluation for the effects of reactivity on the composite morphologies (Table 2). The $(m-p)/p$ values of the nearest neighbor distance between particles were determined to be approximately zero. However, these values of the domain particle diameters were large,

indicating that the distribution deviates significantly from the normal distribution.

The island area fractions decreased well below 69 volume %, which was derived from the design value (wt%) and the densities of the simple acrylic and epoxy elements. These values changed according to the components even though the epoxy thermosetting resin content is the same. This result suggests that the epoxy component could also exist in a high quantity in the sea phase depending on the sample composition.

The differential scanning calorimetry thermograms of the curing process (Figure 6) were acquired at a constant heating rate of $10\text{ }^{\circ}\text{C min}^{-1}$. These thermograms exhibit exothermal behaviors for the heat reaction, and the onset temperature and amount of heat vary with the components. The sample exhibiting a large l_m in Table 3 underwent the heat reaction at a high temperature, which is in agreement with the dependence of the accelerator amount trend. In particular, for the sample MG/E4_1.0, which has the lowest onset temperature and smallest l_m among the samples with the same accelerator amount, the thermal reaction between GMA of MG and the phenol novolac curing agent may suppress phase decomposition and result in a small l_m . Therefore, in these composites, the thermal reaction rate also affects the phase formation.

However, the amount of heat has a high correlation with the amount of covalent bonds formed during heat curing. The MH/E4_1.0 composite exhibits a lower amount of heat (142 J g^{-1}) than that of MA/E4_1.0 (163 J g^{-1}). Therefore, the epoxy thermosetting reactants for MH/E4_1.0 had a lower collision rate than that for MA/E4_1.0 and, therefore, formed fewer covalent bonds.

The shear storage modulus of MH/E4_1.0 at the curing temperature was 1200 Pa , which is lower than that of MA/E4_1.0 (2500 Pa) even though a lower modulus typically provides a high collision rate with highly mobile reactant molecules. Therefore, this lower collision rate of the reactants for MH/E4_1.0 might be caused by chemical interactions via the hydroxyl group of MH.

The ^1H nuclear magnetic resonance FID curves measured by the solid echo and CPMG methods were well represented by equations (1) and (2) ($R^2 > 0.98$), suggesting that the protons in the composites could be divided into one low-mobility and four high-mobility components. The low-mobility components exhibited small T_2 values

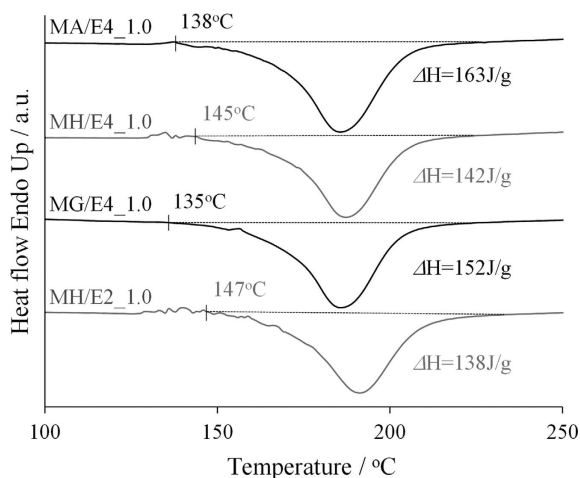


Figure 6 DSC thermograms. The onset temperature and amount of heat are shown in this figure. DSC, differential scanning calorimetry.

(ca. 10^{-2} ms), whereas the high-mobility counterparts exhibited relatively large T_2 values (ca. 10^{-1} – 10^0 ms).

The FID curves of the simple epoxy resin and acrylic polymer were measured using the solid echo and CPMG methods, and were divided into three components, respectively. The largest T_2 obtained for the epoxy resin alone and the smallest T_2 of the acrylic copolymer alone were very close, suggesting that these behaved as one component in the composites. Therefore, the FID curves of the composite were divided into five components. $T_2(1)$, $T_2(2)$ and $T_2(3)$ were attributed to the epoxy thermosetting resins, and $T_2(3)$, $T_2(4)$ and $T_2(5)$ were assigned to the acrylic polymer in the composites.

In addition, the linear combination of the fraction for each proton components in the simple epoxy and acrylic element simulates the complete phase-separated state. The fraction of each T_2 component (F_i (calc)) was derived using the following equation:

$$F_i(\text{calc}) = \begin{cases} f_i(\text{ep}) \times r_{\text{ep}} & (\text{for } i = 1, 2) \\ f_i(\text{ep}) \times r_{\text{ep}} + g_{i-2}(\text{ac}) \times r_{\text{ac}} & (\text{for } i = 3) \\ g_{i-2}(\text{ac}) \times r_{\text{ac}} & (\text{for } i = 4, 5) \end{cases} \quad (8)$$

where $f_i(\text{ep})$ is the fraction obtained for the epoxy thermosetting resin alone and $g_{i-2}(\text{ac})$ is the fraction measured for the acrylic copolymer alone. The index number i corresponds to the number of proton components in the composites, and r_{ep} and r_{ac} are the quantitative proton ratios calculated from the design values for the epoxy resin and acrylic copolymer. The MA/E4_1.0 composite exhibited r_{ep} and r_{ac} values of 0.674 and 0.326, respectively.

The FID curves of the composite were measured, and their fitting results were compared with the linear combinations of individual

Table 4 T_2 and the fraction of each proton component measured by ^1H pulse NMR and the linear sum of each simple element

	$i = 1$	2	3	4	5
<i>MA/E4_1.0</i>					
$T_2(i)$ (ms)	0.016	0.094	0.098	0.73	3.0
$T_2(i)^a$ (ms)	0.015	0.031	0.093	0.17	6.1
F_i (%)	49	7	26	14	4
$F_i(\text{calc})$ (%)	63	3	12 (10) ^b	19	3
<i>MH/E4_1.0</i>					
$T_2(i)$ (ms)	0.016	0.084	0.17	1.0	6.3
$T_2(i)^a$ (ms)	0.015	0.031	0.093	0.18	5.3
F_i (%)	47	14	24	12	3
$F_i(\text{calc})$ (%)	63	3	12 (10) ^b	18	4
<i>MG/E4_1.0</i>					
$T_2(i)$ (ms)	0.015	0.064	0.11	0.64	3.8
$T_2(i)^a$ (ms)	0.015	0.031	0.093	0.25	1.2
F_i (%)	63	19	14	3	1
$F_i(\text{calc})$ (%)	63	3	17 (15) ^b	14	3
<i>MH/E2_1.0</i>					
$T_2(i)$ (ms)	0.014	0.079	0.099	0.67	2.8
$T_2(i)^a$ (ms)	0.014	0.036	0.10	0.18	5.3
F_i (%)	47	8	26	14	5
$F_i(\text{calc})$ (%)	59	6	12 (10) ^b	18	4

Abbreviation: NMR, nuclear magnetic resonance.

^a T_2 value of the simple epoxy thermosetting resin (left half) and the simple acrylic copolymer (right half).

^bThe fraction of the proton component in the acrylic element ($g_{i-2}(\text{ac}) \times r_{\text{ac}}$ in equation (8)) whose index number (i) is 3 (in parentheses).

elements shown in Table 4 to consider the influence of mixing. Rows 1 and 3 list the T_2 and F_1 values that were derived from the FID curves of the composite. Row 2 lists the T_2 values for the epoxy thermosetting resin alone (left half) and acrylic copolymer alone (right half). Row 4 provides the F_1 (calc) values calculated using equation (8). The MA/E4_1.0 composite exhibited a smaller F_1 value (49%; written in a bold-face in Table 4) than F_1 (calc) (63%), which was due to the rigid cured epoxy resins. Therefore, F_3 (26%) surpasses the F_3 (calc) values (12%). This result indicates that the amount of the lower mobility component assigned to the epoxy resin decreased because its mixing with the acrylic copolymer interfered with covalent bond formation during the curing process. The epoxy thermosetting resin did not react fully, and the protons were partly detected as the long-relaxation time ($T_2(3)$) components along with the protons in the acrylic copolymer. However, these $T_2(3)$ values (that is, 0.098 ms; written in a bold-face in Table 4) are smaller than 0.17 ms, which is the $T_2(3)$ value of the simple acrylic copolymer. Therefore, the epoxy resins were sufficiently reactive to influence the acrylic polymer mobility.

Similarly to MA/E4_1.0, the MH/E2_1.0 composite, which contains two types of epoxide resin, exhibited a smaller F_1 than F_1 (calc) and

shorter $T_2(3)$ than its individual components. Although F_1 is the same as F_1 (calc), the MG/E4_1.0 sample exhibited a larger F_2 than F_2 (calc) and a shorter $T_2(3-5)$ than its individual components, suggesting that the glycidyl group in MG reacts with the epoxy thermosetting system to form a covalent bond network. Therefore, the molecular mobility decreased overall.

For the MH/E4_1.0 sample, F_1 decreased, but $T_2(3)$ remains the same as that of the acrylic copolymer alone, indicating that some epoxy resin remained in the acrylic polymer-rich phase and reacted poorly. Therefore, the protons in the epoxy resin may be detected as long-relaxation time ($T_2(3)$) components along with certain protons in acrylic polymer. However, in contrast to the reactivity of the components of MA/E4_1.0, the reactivity of this epoxy resin was too low to affect the acrylic polymer mobility. As a result, $T_2(3)$ did not change from the T_2 value obtained for the acrylic polymer alone. Therefore, the protons in the acrylic polymer retained their mobility in the composite after curing. This decrease in reactivity appears as a reduced amount of heat in differential scanning calorimetry (Figure 6).

The local surface elastic moduli are listed in Table 5. The MA homopolymer and cured epoxy thermosetting system exhibited elastic moduli of 0.88 and 2.9 GPa, respectively. Both the island and sea phases exhibited intermediate values in all of the samples.

In the MA/E4_1.0 and MH/E2_1.0 samples, these average values differ between the island and sea phases as written in a bold-face in Table 5. In general, the number of covalent bonds formed by the epoxy resins influences the elastic modulus. Therefore, the state of the covalent bond network is considered to be different in each phase. However, the s.d. is large. Therefore, the differences in the elastic moduli of each phase are not meaningful adequately. This large s.d. is caused by two reasons. One reason is the sample dimensions with a thickness in which the sea phase exists under the island phase. Another reason involves the incompleteness of the decompose state of the epoxy and acrylic elements. This effect is recognizable because it was also detected as the low intensity of light scattering.

Table 5 Elastic modulus of local sea phase area and local island phase area on the sample surface and the tensile strength at 250 °C (s.d. are in parentheses)

	Elastic modulus of local area (GPa) ^a (s.d.)		Tensile strength at 250°C (MPa) (s.d.)
	Sea phase	Island phase	
MA/E4_1.0	1.96 (0.13)	2.08 (0.19)	0.81 (0.09)
MH/E4_1.0	1.37 (0.05)	1.37 (0.05)	1.20 (0.14)
MG/E4_1.0	1.76 (0.10)	1.76 (0.07)	1.42 (0.12)
MH/E2_1.0	1.91 (0.19)	1.99 (0.17)	1.05 (0.12)

^aThe moduli of simple acrylic polymer and epoxy thermosetting resin are 0.88 and 2.9 GPa, respectively.

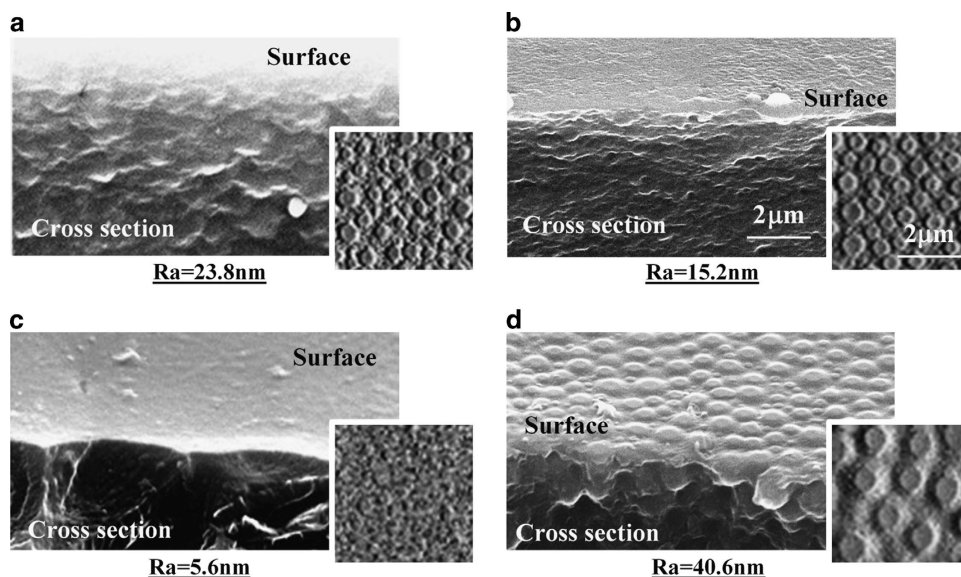


Figure 7 Edge of the cross-section (fracture surface) of the cured film after peel strength test (scanning electron microscopy image). Inset; SPM image (phase mode; same as Figure 2), Number below; Roughness of each cross-section. (a) MA/E4_1.0, (b) MH/E4_1.0, (c) MG/E4_1.0 and (d) MH/E2_1.0.

However, the MH/E4_1.0 and MG/E4_1.0 samples exhibited comparable elastic moduli and small s.d.s in both phases, implying that similar covalent bond networks were formed in both phases.

The tensile strengths at 250 °C are also listed in Table 5. All of the samples exhibited higher tensile strengths than MA/E4_1.0. In particular, the MG/E4_1.0 composite, which has an ambiguous border in the phase-separated structure, exhibited the highest value.

The scanning electron microscopy images of the edge of the cross-section corresponding to the fracture surface after the tensile test are shown in Figure 7. The insets show the surface morphologies at the same magnification, and the figures are the roughness (R_a) of the fracture surface measured by SPM.

The MA/E4_1.0 and MH/E2_1.0 composites exhibited cross-sections resembling their surface morphologies, indicating that the destruction propagates along the phase boundary. By contrast, the MG/E4_1.0 sample exhibited a flat fracture surface and an extremely small R_a value (5.6 nm). Therefore, the destruction may propagate through the island and sea phases.

The planar morphology of the fracture surface is smaller than the domain particle size (0.69 μm , Table 2) in the MH/E4_1.0 composite. This sample exhibited a lower R_a than MA/E4_1.0 despite their quasi-similar particle sizes. This result suggests that the destruction partially propagates through both phases as proposed for MG/E4_1.0. When the destruction propagates through both phases, the fracture surface is smooth, and the tensile strength increases. This mechanism appears to be related to the elastic modulus differences between the phases.

In several previous studies that evaluated the phase separation phenomena and mechanical strength of epoxy composites,^{3,5–7} the sample with a co-continuous phase-separated structure provided an enormously high mechanical strength. However, the similarity of the network in both phases formed by the epoxy thermosetting resin system contributes to mechanical strength enhancement among the samples with the sea-island phase-separated structure. Based on the results of differential scanning calorimetry and pulse ^1H nuclear magnetic resonance, the collision rate of the epoxy reactants is an important factor for network formation and depends on the molecular interactions via covalent and hydrogen bonds.

CONCLUSION

In this study, the phase structure and mechanical properties of acrylic copolymer/epoxy thermosetting resin composites exhibiting the phase separation were evaluated. The SPM morphologies presented sea-island structures wherein the island domains exhibited submicron diameters.

The influence of the epoxy thermosetting resin reactivity on the phase structure was investigated using composites containing different amounts of accelerator. The domain particle size decreased with increasing accelerator content. Thus, the diffusion of the reactants was limited, and the phase decomposition was suppressed by the viscosity increase due to resin polymerization, which results in the termination of structure formation. As a result, the structure of the sample with a high-accelerator content would be nearly fixed prior to sufficient progression of phase separation due to its fast reactivity.

The distribution of the domain particle diameter of the accelerator-rich sample closely approximated a normal Gaussian distribution. However, the domain particle diameter of the accelerator-poor sample exhibited a lognormal distribution. This lognormal distribution resulted from physical quantities obeying the law of proportionate

effect. Therefore, small domains initially formed before accumulating and growing via a phase separation process.

There are peaks in the 1D intensity distribution profiles resulting from the 2D-FFT analysis of the SPM phase images. The samples containing small amounts of accelerator exhibited clearer peaks and longer correlation lengths, suggesting that the structural periodicity and domain size increased with decreasing amount of accelerator. These enhancements were also observed using light scattering measurements of the composites cured under various conditions. These results indicate that the phase-separated structures form via spinodal decomposition. In addition, the thermal reaction of the epoxy resin substantially affects structure formation and serves as a driving force.

The mechanisms governing the mechanical strength enhancement were evaluated by relating the phase structures and their mechanical properties using samples with different compositions. The samples that exhibited small fractions of island area showed similar elastic moduli for their sea and island phases, as well as a low roughness values for their fracture surfaces. Considering that the number of covalent bonds strongly affects the elastic modulus, the epoxy thermosetting system may generate similar networks in both phases, and destruction may propagate through the phases.

When the fracture surface is smooth, the sample provides a high tensile strength. Therefore, the tensile strength increases when the destruction propagates through phases because a considerably higher external force is required to break the boundary area.

Overall, the network structure changes with the composition, and the destruction propagates along or through the phase boundary area depending on the network states in both phases. Controlling these network structures in each phase, taking into account the interaction between the epoxy reactants and other components, is important and contributes to mechanical strength enhancement.

CONFLICT OF INTEREST

The authors declare no conflict of interest.

- 1 JEDEC Standard 22, Method A113F, "Preconditioning of plastic surface mount devices prior to reliability testing". Accessed on October 2008.
- 2 Nakamura, Y., Yamaguchi, M., Tanaka, A. & Okubo, M. Thermal shock test of integrated circuit packages sealed with epoxy moulding compounds filled with spherical silica particles. *Polymer* **34**, 3220–3224 (1993).
- 3 Iwakura, T., Inada, T., Kader, M. A. & Inoue, T. Structure-properties of acrylic rubber/epoxy adhesive by reaction-induced phase decomposition. *J. Soft Mater.* **2**, 13–19 (2006).
- 4 Nunes, S. P. & Inoue, T. Evidence for spinodal decomposition and nucleation and growth mechanisms during membrane formation. *J. Membr. Sci.* **111**, 93–103 (1996).
- 5 Kishi, H., Kunimitsu, Y., Imade, J., Oshita, S., Morishita, Y. & Asada, M. Nano-phase structures and mechanical properties of epoxy/acryl triblock copolymer alloys. *Polymer* **52**, 760–768 (2011).
- 6 Yamanaka, K., Takagi, Y. & Inoue, T. Reaction-induced phase separation in rubber-modified epoxy resins. *Polymer* **30**, 1839–1844 (1989).
- 7 Yamanaka, K. & Inoue, T. Structure development in epoxy resin modified with poly (ether sulphone). *Polymer* **30**, 662–667 (1989).
- 8 Ohnaga, T., Chen, W. & Inoue, T. Structure development by reaction-induced phase separation in polymer mixtures: computer simulation of the spinodal decomposition under the non-isochore depth. *Polymer* **35**, 3774–3781 (1994).
- 9 Shiraishi, T., Motobe, H., Ochi, M., Nakanishi, Y. & Konishi, I. Effect of network structure on thermal and mechanical properties of cured epoxide resins. *Polymer* **33**, 2975–2980 (1992).
- 10 Shimizu, K., Wang, H., Matsuba, G., Wang, Z., Kim, H., Peng, W. & Han, C. C. Interplay of crystallization and liquid-liquid phase separation in polyolefin blends: a thermal history dependence study. *Polymer* **48**, 4226–4234 (2007).
- 11 Rasband, W. S. & ImageJ, N. I. H. ImageJ, NIH <http://imagej.nih.gov/ij/> (1997–2012).
- 12 Schneider, C. A., Rasband, W. S. & Eliceiri, K. W. NIH Image to ImageJ: 25 years of image analysis. *Nat. Methods* **9**, 671–675 (2012).
- 13 Lee, W. I., Loos, A. C. & Spronger, G. S. Heat of reaction, degree of cure, and viscosity of Hercules 3501-6 resin. *J. Compos. Mater.* **16**, 510–520 (1982).

- 14 Powles, J. G. & Strange, J. H. Zero time resolution nuclear magnetic resonance transient in solids. *Proc. Phys. Soc.* **82**, 6–15 (1963).
- 15 Meiboom, S. & Gill, D. Modified spin-echo method for measuring nuclear relaxation times. *Rev. Sci. Instrum.* **29**, 688–691 (1958).
- 16 Tanaka, H. & Nishi, T. Study of block copolymer interface by pulsed NMR. *J. Chem. Phys.* **82**, 4326–4331 (1985).
- 17 Tanaka, H. & Nishi, T. Study of crystallization process of polymer from melt by a real-time pulsed NMR measurement. *J. Chem. Phys.* **85**, 6197–6209 (1986).
- 18 Nakamura, Y., Nishida, Y., Honda, H., Fujii, S. & Sasaki, M. Surface analysis of silanenanolayer on silica particles using ^1H pulse NMR. *J. Adhesion Sci. Technol.* **25**, 2703–2716 (2011).
- 19 Landau, L. D. & Lifshitz, E. M. *Theory of Elasticity: Course of Theoretical Physics, Vol. 7* (Pergamon, New York, NY, USA, 1970).
- 20 Nagai, S. & Fujinami, S. Viscoelastic properties of worm-like micelle of aluminum tristearate/decahydronaphthalene. *Nihon Reoroji Gakkaishi* **36**, 99–106 (2008).
- 21 Colbeck, S. C. Theory of particle coarsening with a log-normal distribution. *Acta Metal* **35**, 1583–1588 (1987).